Microwave surface resistance of potassium in a perpendicular magnetic field: Effects of the charge-density wave

Mi-Ae Park and A. W. Overhauser
Department of Physics, Purdue University, West Lafayette, Indiana 47907
(Received 29 December 1995)

The microwave surface resistance of potassium in a perpendicular magnetic field, measured by Baraff, Grimes, and Platzman in 1969, has never been completely explained until now. The sharp cyclotron resonance peak (at a magnetic field H_c) is caused by the small cylindrical section of Fermi surface created by the charge-density-wave (CDW) minigaps, having periodicities $\vec{K}_n=(n+1)\vec{Q}-n\vec{G}_{110}$. The shape of the observed resonance requires a tilt of the CDW vector $\vec{Q}$ away from [110], predicted by Giuliani and Overhauser in 1979. An abrupt drop of the surface resistance for $|H|>|H_c|$ is caused by the heterodyne gaps, which have periodicities $\vec{K}_n=n(\vec{G}_{110}-\vec{Q})$. These very small gaps, which begin to undergo magnetic breakdown for fields $H>1$ T, interrupt the cyclotron motion of equatorial orbits. The abrupt drop in surface resistance for $|H|>|H_c|$ is caused by the resulting partial loss of carrier effectiveness for electrons having velocities nearly parallel to the surface. [S0163-1829(96)03227-4]

I. INTRODUCTION

Cyclotron resonance of the conduction electrons in potassium was first observed by Grimes and Kip[1] using the Azbel-Kaner configuration,[2] for which the dc magnetic field $\vec{H}$ is parallel to the metal's surface. The effective mass was found to be $m^*=1.21m$. Resonant peaks in the (microwave) surface resistance also occur at subharmonic values,[3] H_c/n, $n=2,3,4,\ldots$, in addition to the fundamental resonance which occurs at $H_c=m^*\omega c/e$. For conduction electrons having an energy spectrum $E(\vec{k})$ that is spherically symmetric, a resonance in the surface resistance should never occur if $\vec{H}$ is perpendicular to the surface.[4]

Nevertheless, Baraff, Grimes, and Platzman, using a perpendicular-field configuration, found a sharp fundamental resonance in the surface resistance of potassium.[5] Their data are shown in Fig. 1 together with the theoretical $R(H)$, which has no resonant structure at all. The magnetic-field sweep, expressed as ω_c/ω (where $\omega/2\pi$ is the microwave frequency, 23.9 GHz, and $\omega_c=eH/m^*c$), includes both positive and negative values because the microwave field was circularly polarized. The sharp cyclotron resonance, at $\omega_c/\omega=-1$, corresponds to $H_c=1.03$ T. Not only was the existence of the resonance unexpected, but the sharp drop of $R(H)$ for $|H|>H_c$ has remained unexplained for twenty-five years.

The reason why a resonance is not expected in a perpendicular field is easily understood. The skin depth is $\sim 10^{-4}$ cm and the Fermi velocity is $\sim 10^8$ cm/s. Accordingly, the time an electron (having the Fermi velocity) remains in the microwave field ($\sim 10^{-12}$ s) is an order of magnitude shorter than the microwave period. (Electrons do not return periodically to the skin depth in a perpendicular field, as occurs if the parallel-field configuration is employed.)

The resonance cannot be an Azbel-Kaner signal from an oblique surface patch (at the sample's edge) since there are no subharmonics. Neither can the resonance be attributed to electrons in a (110) surface-state band, since the bottom of such a band lies ~ 0.45 eV above the Fermi level.

The only satisfactory explanation of the resonance in a perpendicular field is based on the charge-density-wave

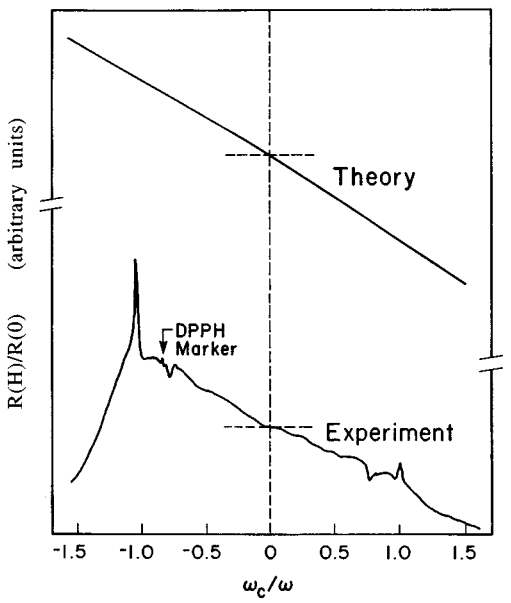

FIG. 1. Surface resistance of potassium versus magnetic field ($\omega_c=eH/m^*c$). The data, due to Baraff, Grimes, and Platzman (Ref. 5), for T = 2.5 K, and circularly polarized radiation at $\omega/2\pi=23.9$ GHz. The dips near ± 0.77 are due to particles of $CuSO_4\cdot 5H_2O$, embedded in the cavity walls during fabrication (Ref. 13). The cyclotron resonance, at $\omega_c/\omega=-1$, occurs when $H=1.03$ T. The small resonance at $\omega_c/\omega=1$ is caused by a small admixture of the opposite polarization. The theoretical curve is for a purely spherical Fermi surface, which potassium would have in the absence of a CDW broken symmetry.

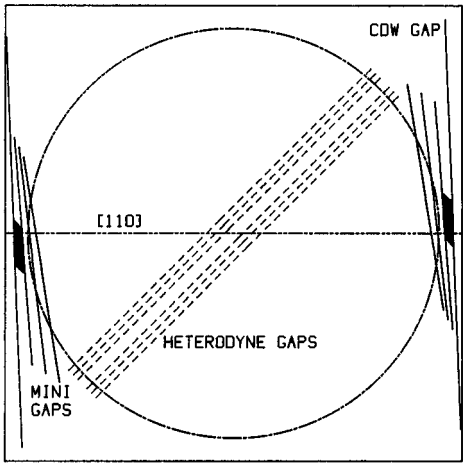

FIG. 2. The Brillouin zone of potassium on a (001) plane in $\vec{k}$ space. The angular tilt, relative to [110], of the CDW wave vector $\vec{Q}$ has been exaggerated for clarity. The minigaps and heterodyne gaps are associated with the periodicities of Eqs. (1) and (2). The shaded areas are the two halves of the Fermi-surface cylinder, which form between the CDW gap and the first minigap. The axis of the cylinder is $\vec{G}_{110}-\vec{Q}$, which is also the direction of the heterodyne-gap vectors. The dc magnetic field $\vec{H}$ is applied parallel to [110], which is the habitual texture direction, perpendicular to smooth potassium surfaces. The (ideal) Fermi sphere is also shown.

(CDW) broken symmetry of potassium.[6] Many anomalous properties (now numbering more than 30) require the presence of a CDW,[7] which causes two sequences of small energy gaps to cut the Fermi surface,[8] as illustrated in Fig. 2. The ''minigaps'' are higher-order gaps created by periodicities:

$$\vec{K}_n=(n+1)\vec{Q}-n\vec{G}_{110} \quad (n=1,2,\ldots), \tag{1}$$

where $\vec{Q}$ is the CDW wave vector and $\vec{G}_{110}$ is the (110) reciprocal lattice vector parallel to $\vec{H}$. (It is known from optical properties that $\vec{Q}$ and one of the {110} reciprocal lattice vectors are nearly perpendicular to a smooth potassium surface.[9]) The calculated values[8] of the first five minigaps are given in Table I.

In Fig. 2 the black regions outline a small cylindrical section of Fermi surface formed by the CDW energy gap and the first minigap. Only a small fraction, $\eta\sim 4\times 10^{-4}$, of the conduction electrons are enclosed by this Fermi-surface cylinder. Nevertheless, these electrons are responsible for the cyclotron-resonance structure in the surface resistance.[10] Landau-level oscillations caused by the cylinder have been observed in microwave transmission.[11] The periodicity of the oscillations (versus $1/H$) indicates that the cylinder radius is $k_F/8$.[12] The small velocities of the cylinder electrons enable them to remain in the microwave skin region and to exhibit a sharp resonance absorption.

TABLE I. Calculated values, from Ref. 8, of the first five minigaps and heterodyne gaps for K. The main CDW gap was taken to be 0.62 eV and the zone-boundary energy gap was 0.40 eV.

n	Minigap (meV)	Heterodyne gap (meV)
1	90	16
2	67	14
3	51	12
4	34	8
5	15	3

The prior treatment of this resonance succeeded in identifying the cylindrical Fermi-surface component as its cause.[10] However, two puzzles remained. The calculated shape of the resonance was antisymmetric rather than (nearly) symmetric. It was possible to ''fix'' this problem by mixing almost equal amounts of surface reactance and surface resistance. A small amount of such mixing could be tolerated experimentally,[13] but the required mixing angle of $\sim 47°$ seems excessive. In Sec. III we will show that this problem disappears when one recognizes that the cylinder's axis is $\sim 45°$ from the [110] (and $\vec{H}$) direction. This axis tilt is required theoretically,[14] and has been verified experimentally by the location of the CDW diffraction satellites.[15] (The cylinder's axis is parallel to $\vec{G}_{110}-\vec{Q}$, which is tilted $\sim 45°$ when $\vec{Q}$ is only $\sim 1°$ away from [110].[8]) The experimental resonance shape can then be ascribed to the surface resistance alone.

The second puzzle is the sharp drop in $R(H)$ for $|H|>H_c$, mentioned above. In the following section, we will show that this effect arises from the ''heterodyne'' gaps, created by the periodicities,

$$\vec{K}_n=n(\vec{G}_{110}-\vec{Q}) \quad (n=1,2,\ldots). \tag{2}$$

The energy-gap planes of this family are shown by the dashed lines in Fig. 2, which cut at an angle, $\sim 45°$, through the central region of the Fermi ''sphere.'' The calculated values[8] of the first five heterodyne gaps are given in Table I. Cyclotron orbits for which k_z is near zero can be ''Bragg'' reflected by the periodic potentials associated with $\{\vec{K}_n\}$, Eq. (2). When such reflections occur, the electrons become ''ineffective'' with regard to their cyclotron rotation. A quantitative model for this phenomenon is presented in Sec. II; and the observed behavior of $R(H)$ when $|H|>|H_c|$ is explained.

II. EFFECT OF THE HETERODYNE GAPS

In this section we will develop a model to account for the disruption of cyclotron motion caused by the heterodyne gaps, which cut through the central section of the Fermi sphere, as shown by the dashed lines in Fig. 2. (The dc magnetic field $\vec{H}$ is parallel to the horizontal, $\hat{z}$ axis.) The main contribution to the surface resistance $R(H)$ arises from electrons having velocities nearly parallel to the surface; so these electrons (with $k_z\sim 0$) necessarily encounter the heterodyne gaps.

An electron which meets a heterodyne gap during its cyclotron motion can suffer a momentum transfer $\pm\hbar\vec{K}_n$, given by Eq. (2). The result is a disruption of its cyclotron motion (in the $\hat{x}\hat{y}$ plane); and the change in $\hat{z}$ component of its velocity can cause it to rapidly leave the microwave skin depth, so its cyclotron motion is no longer fully effective.

We introduce a factor $f<1$ which describes the probability that the electron behaves ''effectively,'' i.e., as if there were no gaps.

An electron encountering a small energy gap can also continue on its path in $\vec{k}$ space, as it would if the gap were not present. This phenomenon is called ''magnetic breakdown.'' The breakdown probability P depends exponentially on H:[16]

$$P=e^{-H_0/H}. \tag{3}$$

The parameter H_0 depends critically on the energy gap E_g and the orbit geometry:

$$H_0=\frac{\pi mcE_g^2}{2\hbar^2 e|\vec{K}\cdot(\vec{v}\times\hat{H})|}, \tag{4}$$

where $\hat{H}$ is a unit vector parallel to $\vec{H}$, and $\vec{v}$ is the electron's velocity at the energy-gap plane (if E_g were zero). This invariant form[17] for H_0 is equivalent to the result derived by Blount.[16] It is clear from Fig. 2 that an electron with $k_z\sim 0$ will encounter several heterodyne gaps. For simplicity, we will still employ Eq. (3) to describe the net result of all such encounters. The effective fraction, on taking into account magnetic breakdown, is then

$$f_{\rm eff}(k_z=0)=f+(1-f)e^{-H_0/H}. \tag{5}$$

At very high fields, when magnetic breakdown is complete, $f_{\rm eff}=1$, i.e., the electrons behave as they would without a CDW. For small H, $f_{\rm eff}=f$, the parameter we introduced above, f, a constant, will be adjusted to fit the data. (f is not zero because electrons with $k_z\sim 0$ sustain part of their cyclotron motion.) On account of the complexity, the breakdown parameter H_0 cannot be calculated reliably; but we have estimated it to be $H_0\sim 4$ T.

Equation (5) applies only to orbits for which $k_z\sim 0$; so we must generalize the effective fraction for all k_z. Electrons having a rapid speed along $\hat{z}$ do not remain in the skin layer very long anyway, so the interruption of their $\hat{x}\hat{y}$ motion by the heterodyne gaps is of little consequence. Thus their effectiveness will approach unity as $|k_z|$ increases. This behavior can be described heuristically by

$$f_{\rm eff}(k_z)=\frac{f+(1-f)e^{-H_0/H}+\beta|k_z/k_F|}{1+\beta|k_z/k_F|}. \tag{6}$$

The constant β will be adjusted to fit the surface-resistance data. The fitted values are $f=0.8$ and $\beta=20$. It is clear that $f_{\rm eff}$ approaches unity rapidly as k_z becomes appreciable; and (of course) $f_{\rm eff}$ equals Eq. (5) when $k_z=0$.

The foregoing ideas are needed to correct the theoretical electron-gas conductivity, $\sigma_{\alpha\beta}(q,\omega)$, which is obtained by solving the Boltzmann transport equation. For an isotropic, free-electron metal the solution is standard. However, we display σ_{xx} and σ_{xy}, the components derived from Eqs. (12) and (13) of Ref. 10:

$$\sigma_{xx}=\frac{3\sigma_0}{8}\int_{-1}^{1}dt(1-t^2)\left[\frac{1}{1-ia_++ixt}+\frac{1}{1-ia_-+ixt}\right],$$

$$\sigma_{xy}=\frac{3i\sigma_0}{8}\int_{-1}^{1}dt(1-t^2)\left[\frac{1}{1-ia_++ixt}-\frac{1}{1-ia_-+ixt}\right], \tag{7}$$

where

$$\sigma_0=\frac{ne^2\tau}{m^*},$$

$$a_+\equiv(\omega+\omega_c)\tau,$$

$$a_-\equiv(\omega-\omega_c)\tau,$$

$$x\equiv ql=qv_F\tau,$$

$$t\equiv\frac{k_z}{k_F}. \tag{8}$$

τ is the scattering time, and the magnetic field H (parallel to $\hat{z}$) appears linearly in ω_c, the cyclotron frequency, eH/m^*c. The Cartesian components of σ are displayed here, instead of the circularly polarized ones, to anticipate the requirements of Sec. III.

Notice that the factor $(1-t^2)$ in the integrand of Eq. (7) is proportional to the cross-sectional area of the Fermi surface for $t=k_z/k_F$, i.e., to the number of electrons in the slice of width dt. However, as argued above, the heterodyne gaps reduce the effective number by the factor Eq. (6). Consequently, we must replace

$$(1-t^2)\rightarrow(1-t^2)f_{\rm eff}(k_z), \tag{9}$$

when the integrals are evaluated. Fortunately, these integrals can be found analytically because, as is evident in what follows, the surface resistance involves a further integration over the wave vector q, which can only be carried out numerically. The analytic expressions for σ_{xx} and σ_{xy} which incorporate the substitution Eq. (9) are given in Appendix A.

Now, the surface impedance Z for an isotropic metal, having an $\hat{x}\hat{y}$ surface at $z=0$, is defined by

$$Z=\frac{\mathcal{E}_x(0)}{\int_0^\infty j_x(z)dz}. \tag{10}$$

With the use of Stoke's theorem for a circuit in the $\hat{y}\hat{z}$ plane and the two Maxwell curl equations,

$$\mathcal{E}_x'(0)=\frac{4\pi i\omega}{c^2}\int_0^\infty j_x(z)dz. \tag{11}$$

The prime indicates $\partial/\partial z$, and the time dependence of the fields is taken as $\exp(-i\omega t)$. It follows that

$$Z=\frac{4\pi i\omega}{c^2}\frac{\mathcal{E}_x(0)}{\mathcal{E}_x'(0)}. \tag{12}$$

Solution of Maxwell's equations in the metal with specular boundary conditions at $z=0$ can be found in Ref. 18, which we follow. For the $\alpha=\hat{x},\hat{y}$ components of polarization,

$$\frac{d^2\mathcal{E}_\alpha(z)}{dz^2}+\frac{\omega^2}{c^2}\mathcal{E}_\alpha(z)=-\frac{4\pi i\omega}{c^2}j_\alpha(z). \tag{13}$$

Solution of this equation may be obtained by Fourier transform. It has been shown experimentally[19] that conduction electrons are specularly reflected from shiny potassium surfaces. Under these conditions, one can treat the metal as infinite, instead of semi-infinite, provided $\mathcal{E}(z)$ is extended symmetrically to the region $z<0$. This means that at $z=0$, $\mathcal{E}'$ must undergo a jump from $-\mathcal{E}'(0)$ to $\mathcal{E}'(0)$. Accordingly, integration by parts gives

$$\int_{-\infty}^{\infty}\mathcal{E}''e^{-iqz}dz=\left(\int_{-\infty}^{-0}+\int_{+0}^{\infty}\right)\mathcal{E}''e^{-iqz}dz$$
$$=-2\mathcal{E}'(0)-q^2E(q). \tag{14}$$

The Fourier transform of Eq. (13) is then

$$\left(-q^2+\frac{\omega^2}{c^2}\right)E_\alpha(q)=-\frac{4\pi i\omega}{c^2}J_\alpha(q)+\sqrt{\frac{2}{\pi}}\mathcal{E}'_\alpha(0), \tag{15}$$

where for each component, $\alpha=x,y$,

$$E(q)=\frac{1}{\sqrt{2\pi}}\int_{-\infty}^{\infty}\mathcal{E}(z)e^{-iqz}dz, \tag{16}$$

$$J(q)=\frac{1}{\sqrt{2\pi}}\int_{-\infty}^{\infty}j(z)e^{-iqz}dz,$$

$$\mathcal{E}(z)=\frac{1}{\sqrt{2\pi}}\int_{-\infty}^{\infty}E(q)e^{iqz}dq,$$

$$j(z)=\frac{1}{\sqrt{2\pi}}\int_{-\infty}^{\infty}J(q)e^{iqz}dq.$$

Equation (15) is actually a pair of coupled equations because the conductivity tensor (7) has off-diagonal components. On using σ_{ij} to eliminate $J_\alpha(q)$, Eq. (15) becomes

$$D_{ij}(q,\omega)E_j(q)=-\sqrt{\frac{2}{\pi}}\mathcal{E}'_i(0), \tag{17}$$

where

$$D_{ij}(q,\omega)\equiv\begin{pmatrix} q^2-\frac{\omega^2}{c^2}-\frac{4\pi i\omega}{c^2}\sigma_{xx} & -\frac{4\pi i\omega}{c^2}\sigma_{xy} \\ -\frac{4\pi i\omega}{c^2}\sigma_{yx} & q^2-\frac{\omega^2}{c^2}-\frac{4\pi i\omega}{c^2}\sigma_{yy}\end{pmatrix}. \tag{18}$$

For a spherical Fermi surface, $\sigma_{xx}=\sigma_{yy}$ and $\sigma_{yx}=-\sigma_{xy}$. Equation (17) can then be solved:

$$E_x(q)=-\sqrt{\frac{2}{\pi}}\frac{[q^2-\omega^2/c^2-(4\pi i\omega/c^2)\sigma_{xx}]\mathcal{E}'_x(0)+(4\pi i\omega/c^2)\sigma_{xy}\mathcal{E}'_y(0)}{[q^2-\omega^2/c^2-(4\pi i\omega/c^2)\sigma_{xx}]^2+[(4\pi i\omega/c^2)\sigma_{xy}]^2}. \tag{19}$$

We now introduce circularly polarized waves accordingly to the convention

$$\vec{\mathcal{E}}_\pm(z)=(\hat{x}\pm i\hat{y})\mathcal{E}_\pm(0)e^{i(qz-\omega t)}. \tag{20}$$

It follows that

$$\mathcal{E}'_y(0)=\pm i\mathcal{E}'_x(0). \tag{21}$$

This relation allows one to solve Eq. (19) for $E_x(q)/\mathcal{E}'_x(0)$. Subsequently, the third relation of Eq. (16), with $z=0$, can be used to find $\mathcal{E}_x(0)/\mathcal{E}'_x(0)$, which is all one needs to evaluate the surface impedance (12). The final result is, after restricting the integration to positive q,

$$Z_\pm(H)=-8i\omega\int_0^\infty\frac{dq}{c^2q^2-\omega^2-4\pi i\omega(\sigma_{xx}\pm i\sigma_{xy})}. \tag{22}$$

[That the integrand is even in q follows from the symmetry of $\mathcal{E}(z)$ mentioned above.] The integration in dq must be carried out numerically with the expressions for σ_{xx} and σ_{xy} from Appendix A. It was found sufficient to sum from $q=0$ to 500 000 in 50 000 steps. (Doubling the range or reducing the step size by 10 did not alter the output noticeably.)

Inspection of the experimental data of Fig. 1 reveals that the cavity was not driven in a pure ''$-$'' mode. Accordingly, we have calculated the surface resistance given by

$$R(H)=\mathrm{Re}[0.8Z_-(H)+0.2Z_+(H)]. \tag{23}$$

The residual-resistance ratio of potassium, $\rho(300K)/\rho(4\ \mathrm{K})$, is typically $\sim$5000. This value implies a scattering time $\tau\sim2\times10^{-10}$ s. For 23.9 GHz, $\omega\tau=30$. $R(H)$ calculated from Eq. (23) is shown in Fig. 3. The heterodyne gaps cause the surface resistance to decrease when $|H|>H_c$ and to level off near $|\omega_c/\omega|\sim2$. Not shown is the eventual recovery of $R(H)$ to the ideal Fermi-sphere result for $|\omega_c/\omega|>3$. The rate of this high-field approach to the ideal $R(H)$ depends on the magnetic-breakdown parameter H_0; so H_0 can in principle be estimated by studying $R(H)$ in the high-field regime. Baraff has reported[20] that unpublished data of Grimes do indeed show the recovery of $R(H)$ just described. (We have not seen these particular data.)

Interruption of the cyclotron motion for electrons having $k_z\sim0$, caused by the heterodyne gaps, reproduces the observed behavior of $R(H)$ when $|H|>H_c$. The sharp peaks at cyclotron resonance, however, are caused by the cylindrical section of Fermi surface shown in Fig. 2, and will be explained below. The observed resonance dips near $\omega_c/\omega=\pm0.77$ have nothing to do with the potassium

sample. They are caused by embedded particles of $Cu_2SO_4 \cdot 5H_2O$ in the cavity walls created during fabrication.[13]

III. RESONANCE FROM THE FERMI-SURFACE CYLINDER

The minigaps, shown by the short, solid lines in Fig. 2, correspond to the periodicities of Eq. (1). The sizes of the first few minigaps,[8] tabulated in Table I, are substantial. The two black patches in Fig. 2 represent a small Fermi-surface cylinder which forms between the first minigap and the main CDW gap (having periodicity $\vec{Q}$). It has already been shown[10] that such a cylinder can explain the occurrence of the sharp cyclotron resonance observed by Baraff, Grimes, and Platzman and reproduced in Fig. 1.

The size of the resonance requires the volume of the cylinder (pieced together from the two halves) to be a very small fraction, $\eta \sim 4\times10^{-4}$, of the Fermi-sphere volume. It is noteworthy that this volume fraction agrees with the value calculated from the product of the cylinder's length and its cross-sectional area. The former is obtained from the neutron-diffraction measurement of $\vec{Q}$,[15] and the latter from the periodicity of the Landau-level oscillations,[12] observed in microwave transmission.[11] The cylinder's radius is $k_c = k_F/8$, and its length (projected along [110]) is $0.015 G_{110}$. Although $\vec{Q}$ is tilted from [110] by about 1°, the cylinder's axis, $\vec{Q}' \equiv \vec{G}_{110} - \vec{Q}$, is tilted about 45° from [110],

$$\vec{Q}' \approx (0.025, 0.015, 0.005)\frac{2\pi}{a}. \tag{24}$$

Its cross section is approximately circular in a plane perpendicular to [110].

It is of interest to calculate first the surface resistance $R(H)$ caused by a cylinder having its axis parallel to the magnetic field $\vec{H}$. On account of the cylinder's small size, electron velocities on the Fermi surface of the cylinder are also small. Accordingly, we will use a local conductivity tensor for the cylinder. The dc conductivity in the $\hat{x}\hat{y}$ plane is $\eta\sigma_{0c}$ and $\sigma_{zz}=0$, where σ_{0c} is $ne^2\tau_c/m^*$. The sharpness of the observed resonance corresponds to $\omega\tau_c \sim 150$. That τ_c (on the cylinder) should be ~ 5 times larger than τ on the main Fermi surface is reasonable because of the smaller velocities of the cylinder electrons. The cylinder's conductivity tensor is then

$$\sigma^{\rm cyl} = \frac{\eta\sigma_{0c}}{(1-i\omega\tau_c)^2+(\omega_c\tau_c)^2}\begin{pmatrix} 1-i\omega\tau_c & -\omega_c\tau_c & 0 \\ \omega_c\tau_c & 1-i\omega\tau_c & 0 \\ 0 & 0 & 0 \end{pmatrix}. \tag{25}$$

For this exercise we will neglect the effect of the heterodyne gaps. Consequently, $\sigma^{\rm cyl}$, Eq. (25), is added to the conductivity, Eq. (7), for an ideal Fermi sphere. The surface impedance is still given by Eq. (22), and $R(H)$ for 80% circular polarization is obtained from (23). The result is shown in Fig. 4 with $\omega\tau_c = 150$. A sharp cyclotron resonance is obtained but, unlike the data of Fig. 1, the shape is asymmetric.

The sharp, asymmetric resonance shown in Fig. 4 was obtained previously,[10] but the remedy attempted then involved introduction of a more than 50-50 admixture of surface reactance and surface resistance. However, a remedy not involving such an admixture is possible. Since the cylinder's axis must, theoretically, be tilted $\sim 45°$ from [110],[14] an angle confirmed by neutron diffraction,[15] we now study the effect of such a tilt on the resonance shape.

The equation for a cylindrical surface of constant energy $\epsilon = E_F$, having an axis at an angle θ relative to the direction of $\vec{H}$, and with $\vec{k}$ relative to the cylinder's center, is

$$\epsilon - \epsilon_0 = \frac{\hbar^2}{2m^*}[(k_x - k_z\tan\theta)^2 + k_y^2]. \tag{26}$$

This cylinder has a circular cross section in the $\hat{x}\hat{y}$ plane. Consequently, the cyclotron frequency, with $\vec{H}$ along $\hat{z}$, is unchanged. (For the cylinder of interest here, $\epsilon - \epsilon_0 = E_F/64$.) On account of its small size, as already discussed, the electron velocities on this surface are $\sim v_F/8$. We will therefore employ local equations of motion to find the tilted cylinder's conductivity tensor $\sigma^{\rm cyl}$. The Lorentz equation for motion in the electric and magnetic fields is

$$\vec{v} = -eM^{-1}(\vec{k})\left[\vec{\mathcal{E}} + \frac{1}{c}\vec{v}\times\vec{H}\right] - \frac{\vec{v}}{\tau_c}, \tag{27}$$

where $\hbar\vec{v} = \nabla_k\epsilon(\vec{k})$, and the effective mass tensor is

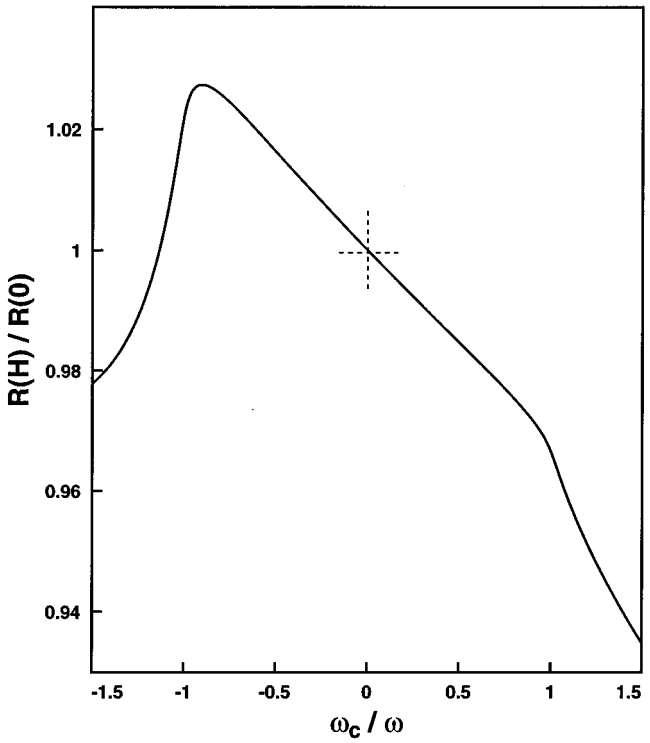

FIG. 3. Theoretical surface resistance for a Fermi sphere having only heterodyne-gap intersections. The parameters of Eq. (6), which quantify the loss in effective cyclotron motion on equatorial orbits, are $f=0.8$ and $\beta=20$. The drop in R for $|H|>H_c$ increases with decreasing f. The steepness of the decline increases with increasing β. The magnetic-breakdown field is $H_0=4$ T. The electron scattering time corresponds to $\omega\tau=30$.

$$[M^{-1}(\vec{k})]_{ij}=\frac{1}{\hbar^2}\frac{\partial^2\epsilon(\vec{k})}{\partial k_i\partial k_j}. \tag{28}$$

Then

$$v_x=\frac{\hbar}{m^*}(k_x-k_z\tan\theta), \tag{29}$$

$$v_y=\frac{\hbar}{m^*}k_y,$$

$$v_z=-\frac{\hbar}{m^*}(k_x-k_z\tan\theta)\tan\theta.$$

Equations (26)–(29) can now be used to find the conductivity of the cylinder:

$$\sigma^{\rm cyl}=\frac{\eta\sigma_{0c}}{(1-i\omega\tau_c)^2+(\omega_c\tau_c)^2}\begin{pmatrix} 1-i\omega\tau_c & -\omega_c\tau_c & -\tan\theta(1-i\omega\tau_c) \\ \omega_c\tau_c & 1-i\omega\tau_c & -\tan\theta(\omega_c\tau_c) \\ -\tan\theta(1-i\omega\tau_c) & \tan\theta(\omega_c\tau_c) & \tan^2\theta(1-i\omega\tau_c)\end{pmatrix}. \tag{30}$$

After comparing this tensor with Eq. (25), for which $\theta=0$, it is clear that the electric field may now have a longitudinal, $\hat{z}$ component. J_x and J_y of Eq. (15) now involve $\mathcal{E}_z$ because σ_{xz} and σ_{yz} are no longer zero. However, we can express $\mathcal{E}_z$ in terms of $\mathcal{E}_x$ and $\mathcal{E}_y$ by using the requirement that the total longitudinal current J_z be zero everywhere. Accordingly,

$$J_z(q)=\sigma_{zx}^{\rm cyl}E_x+\sigma_{zy}^{\rm cyl}E_y+(\sigma_{zz}^{\rm sph}+\sigma_{zz}^{\rm cyl})E_z=0. \tag{31}$$

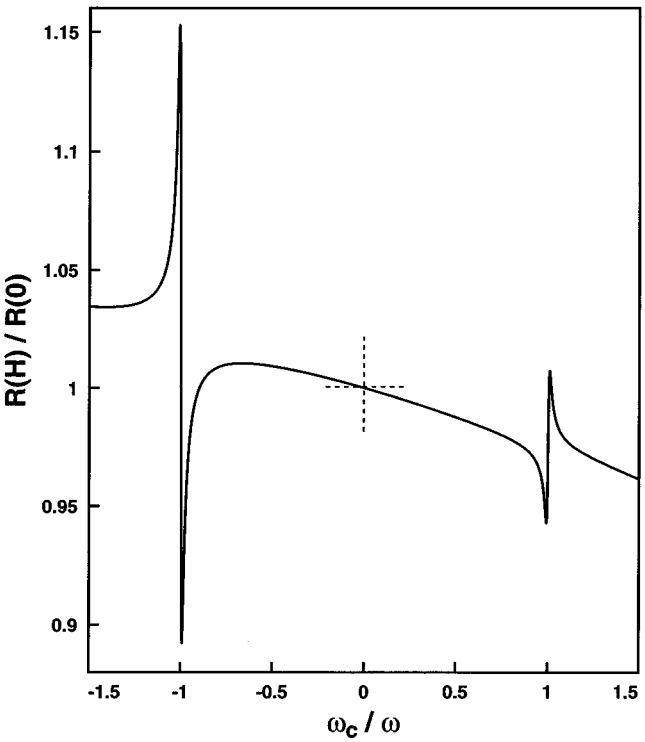

FIG. 4. Theoretical surface resistance of conduction electrons having $\omega\tau=30$ on the Fermi sphere and $\omega\tau_c=150$ on the Fermi-surface cylinder (containing $\sim 4\times10^{-4}$ electrons per atom). The axis of the cylinder is, here, parallel to $\vec{H}$, and the heterodyne gaps (intersecting the sphere) are ignored. A 4:1 ratio of left to right circular polarization is assumed.

The longitudinal conductivity of the spherical portion of the Fermi surface must be calculated nonlocally using the Boltzmann transport equation. For a longitudinal electric field, proportional to $e^{iqz-i\omega t}$,

$$\sigma_{zz}^{\rm sph}=\frac{3\sigma_0}{2}\int_{-1}^{1}dt\frac{t^2}{1-i\omega\tau+ixt}$$

$$=\frac{3\sigma_0}{2x^3}[2x-r+2\omega\tau p+\omega^2\tau^2 r+i(p-2\omega\tau x$$

$$+2\omega\tau r-\omega^2\tau^2 p)], \tag{32}$$

with

$$p=\frac{1}{2}\ln\left[\frac{1+(x-\omega\tau)^2}{1+(x+\omega\tau)^2}\right],$$

$$r=\tan^{-1}(x-\omega\tau)+\tan^{-1}(x+\omega\tau). \tag{33}$$

Equation (31) together with Eq. (15) changes Eq. (17) as follows:

$$\left[q^2-\frac{\omega^2}{c^2}-\frac{4\pi i\omega}{c^2}\left(\sigma_{xx}-\frac{\sigma_{xz}\sigma_{zx}}{\sigma_{zz}}\right)\right]E_x$$

$$-\frac{4\pi i\omega}{c^2}\left(\sigma_{xy}-\frac{\sigma_{xz}\sigma_{zy}}{\sigma_{zz}}\right)E_y$$

$$=-\sqrt{\frac{2}{\pi}}\mathcal{E}_x'(0),$$

$$-\frac{4\pi i\omega}{c^2}\left(\sigma_{yx}-\frac{\sigma_{yz}\sigma_{zx}}{\sigma_{zz}}\right)E_x+\left[q^2-\frac{\omega^2}{c^2}\right.$$

$$\left.-\frac{4\pi i\omega}{c^2}\left(\sigma_{yy}-\frac{\sigma_{yz}\sigma_{zy}}{\sigma_{zz}}\right)\right]E_y$$

$$=-\sqrt{\frac{2}{\pi}}\mathcal{E}_y'(0), \tag{34}$$

where $\sigma_{ij}=\sigma_{ij}^{\rm sph}+\sigma_{ij}^{\rm cyl}$. These two equations can be expressed compactly:

$$D_{ij}(q,\omega)E_j(q) = -\sqrt{\frac{2}{\pi}}\mathcal{E}'_i(0) \tag{35}$$

with

$$D_{ij}(q,\omega) \equiv \begin{pmatrix} q^2 - \frac{\omega^2}{c^2} - \frac{4\pi i\omega}{c^2}\sigma'_{xx} & -\frac{4\pi i\omega}{c^2}\sigma'_{xy} \\ -\frac{4\pi i\omega}{c^2}\sigma'_{yx} & q^2 - \frac{\omega^2}{c^2} - \frac{4\pi i\omega}{c^2}\sigma'_{yy} \end{pmatrix}. \tag{36}$$

Here,

$$\sigma'_{ij} = \sigma_{ij} - \frac{\sigma_{iz}\sigma_{zj}}{\sigma_{zz}}. \tag{37}$$

i and j denote x or y. The difference between Eq. (36) and Eq. (18) of Sec. II is that all transverse conductivities σ_{ij} in Eq. (18) are replaced by σ'_{ij} in Eq. (36). For example, σ'_{xx} includes σ_{xz}, σ_{zx}, and σ_{zz} as well as σ_{xx}. The longitudinal motion of electrons in the cylinder leads to creation of an electric field in the $\hat{z}$ direction. The $\mathcal{E}_z$ which arises (to preserve charge neutrality) plays a role in producing the transverse currents j_x and j_y due to the nonzero values of σ_{xz} and σ_{yz}. (The tilted Fermi-surface cylinder mixes the transverse and longitudinal motions.) Even though the number of electrons in the cylinder is small, this mixing causes a large change in the surface impedance. The total conductivity tensor has the following properties:

$$\sigma_{yx} = -\sigma_{xy}, \quad \sigma_{zy} = -\sigma_{yz}, \quad \sigma_{zx} = \sigma_{xz}. \tag{38}$$

Accordingly, from Eq. (37), $\sigma'_{yx} = -\sigma'_{xy}$. Equation (35) may now be solved:

$$E_x(q) = -\sqrt{\frac{2}{\pi}}\frac{(q^2c^2-\omega^2-4\pi i\omega\sigma'_{yy})\mathcal{E}'_x(0) + 4\pi i\omega\sigma'_{xy}\mathcal{E}'_y(0)}{(q^2c^2-\omega^2-4\pi i\omega\sigma'_{xx})(q^2c^2-\omega^2-4\pi i\omega\sigma'_{yy}) + (4\pi i\omega\sigma'_{xy})^2},$$

$$E_y(q) = -\sqrt{\frac{2}{\pi}}\frac{-4\pi i\omega\sigma'_{xy}\mathcal{E}'_x(0) + (q^2c^2-\omega^2-4\pi i\omega\sigma'_{xx})\mathcal{E}'_y(0)}{(q^2c^2-\omega^2-4\pi i\omega\sigma'_{xx})(q^2c^2-\omega^2-4\pi i\omega\sigma'_{yy}) + (4\pi i\omega\sigma'_{xy})^2}. \tag{39}$$

Using Eq. (11), we express $\mathcal{E}'_i(0)$ in terms of the total current density J_i,

$$J_i = \int_0^\infty j_i(z)dz. \tag{40}$$

The third equation of (16), together with (38)–(40), give the electric field at $z = 0$:

$$\mathcal{E}_x(0) = -\frac{8i\omega}{c^2}\int_0^\infty dq \frac{(q^2c^2-\omega^2-4\pi i\omega\sigma'_{yy})J_x + 4\pi i\omega\sigma'_{xy}J_y}{(q^2c^2-\omega^2-4\pi i\omega\sigma'_{xx})(q^2c^2-\omega^2-4\pi i\omega\sigma'_{yy}) + (4\pi i\omega\sigma'_{xy})^2},$$

$$\mathcal{E}_y(0) = -\frac{8i\omega}{c^2}\int_0^\infty dq \frac{-4\pi i\omega\sigma'_{xy}J_x + (q^2c^2-\omega^2-4\pi i\omega\sigma'_{xx})J_y}{(q^2c^2-\omega^2-4\pi i\omega\sigma'_{xx})(q^2c^2-\omega^2-4\pi i\omega\sigma'_{yy}) + (4\pi i\omega\sigma'_{xy})^2}. \tag{41}$$

These expressions can be written compactly:

$$\mathcal{E}_x(0) = Z_{xx}J_x + Z_{xy}J_y,$$

$$\mathcal{E}_y(0) = -Z_{xy}J_x + Z_{yy}J_y, \tag{42}$$

which by inspection of (41) defines the four components of $Z_{\alpha\beta}$, the surface impedance tensor.

It is clear from Eqs. (40) and (41) that J_α ($\alpha = x,y$) depend intricately on the bulk electric fields. Anisotropy caused by the cylinder's tilt causes J_α to be a complicated function of the conductivity components. This asymmetry also prevents the field from having perfect circular polarization. This behavior is studied in Appendix B. Nevertheless, on account of the small size of the cylinder, the electric-field polarization is almost circular. Accordingly,

$$H_y(0) \approx \pm iH_x(0),$$

$$J_y \approx \pm iJ_x. \tag{43}$$

The electric field at the surface will be $\mathcal{E}_x = \mathcal{E}_0 e^{-i\omega t}$ and $\mathcal{E}_y = i\mathcal{E}_x$, which corresponds to right circular polarization. ($\mathcal{E}_0$ is real.) Then from Eq. (B25),

$$J_x = \frac{c\mathcal{E}_0}{2\pi}e^{-i\omega t},$$

$$J_y = i\frac{c\mathcal{E}_0}{2\pi}e^{-i\omega t}. \tag{44}$$

The power absorbed per unit area per unit time is

$$S_z=\frac{c}{4\pi}\{\mathrm{Re}[\vec{\mathcal{E}}(0)]\times\ \mathrm{Re}[\vec{H}(0)]\}_z$$

$$=\frac{c}{4\pi}\{\mathrm{Re}[\mathcal{E}_x(0)]\mathrm{Re}[H_y(0)]-\ \mathrm{Re}[\mathcal{E}_y(0)]\mathrm{Re}[H_x(0)]\}$$

$$=\mathrm{Re}[\mathcal{E}_x(0)]\mathrm{Re}[J_x]+\mathrm{Re}[\mathcal{E}_y(0)]\ \mathrm{Re}[J_y]. \tag{45}$$

We now separate $Z_{\alpha\beta}$ [defined by (41) and (42)] into their real and imaginary parts, i.e.,

$$Z_{\alpha\beta}=R_{\alpha\beta}+iI_{\alpha\beta}, \tag{46}$$

where $R_{\alpha\beta}$ is the real part of $Z_{\alpha\beta}$ and $I_{\alpha\beta}$ its imaginary part. It follows that

$$\mathrm{Re}(J_x)=\frac{c\mathcal{E}_0}{2\pi}\cos(\omega t), \tag{47}$$

$$\mathrm{Re}(J_y)=\frac{c\mathcal{E}_0}{2\pi}\sin(\omega t),$$

$$\mathrm{Re}(\mathcal{E}_x)=\frac{c\mathcal{E}_0}{2\pi}[R_{xx}\cos(\omega t)+I_{xx}\sin(\omega t)+R_{xy}\sin(\omega t)$$

$$-I_{xy}\cos(\omega t)],$$

$$\mathrm{Re}(\mathcal{E}_y)=\frac{c\mathcal{E}_0}{2\pi}[R_{yy}\sin(\omega t)-I_{yy}\cos(\omega t)-R_{xy}\cos(\omega t)$$

$$-I_{xy}\sin(\omega t)].$$

By using these expressions in Eq. (45) and averaging over time, we find the absorbed power.

$$\overline{S_z}=\overline{\mathrm{Re}[\mathcal{E}_x(0)]\mathrm{Re}[J_x]+\ \mathrm{Re}[\mathcal{E}_y(0)]\mathrm{Re}[J_y]}$$

$$=\frac{c^2\mathcal{E}_0^2}{8\pi^2}(R_{xx}+R_{yy}-2I_{xy})$$

$$=\frac{c^2\mathcal{E}_0^2}{4\pi^2}\mathrm{Re}[\tfrac{1}{2}(Z_{xx}+Z_{yy})+iZ_{xy}]. \tag{48}$$

The effective surface resistance is therefore

$$R=\mathrm{Re}[\tfrac{1}{2}(Z_{xx}+Z_{yy})+iZ_{xy}]. \tag{49}$$

From Eqs. (41) and (42), and $\mathcal{E}_y=i\mathcal{E}_x$ for right circular polarization, the surface impedance is

$$Z_R=\frac{1}{2}(Z_{xx}+Z_{yy})+iZ_{xy}=-\frac{8i\omega}{c^2}\int_0^\infty dq\,\frac{[q^2c^2-\omega^2-2\pi i\omega(\sigma'_{xx}+\sigma'_{yy})]-4\pi\omega\sigma'_{xy}}{(q^2c^2-\omega^2-4\pi i\omega\sigma'_{xx})(q^2c^2-\omega^2-4\pi i\omega\sigma'_{yy})+(4\pi i\omega\sigma'_{xy})^2}. \tag{50}$$

For a left circularly polarized wave on the front surface, i.e., $\mathcal{E}_y=-i\mathcal{E}_x$, the surface impedance is

$$Z_L=\frac{1}{2}(Z_{xx}+Z_{yy})-iZ_{xy}=-\frac{8i\omega}{c^2}\int_0^\infty dq\,\frac{[q^2c^2-\omega^2-2\pi i\omega(\sigma'_{xx}+\sigma'_{yy})]+4\pi\omega\sigma'_{xy}}{(q^2c^2-\omega^2-4\pi i\omega\sigma'_{xx})(q^2c^2-\omega^2-4\pi i\omega\sigma'_{yy})+(4\pi i\omega\sigma'_{xy})^2}. \tag{51}$$

Equations (50) and (51) must be evaluated numerically, as in Sec. II. The effective surface resistance applicable to the experiment, for which the polarization was about a 4:1 admixture of L and R, is now

$$R(H)=\mathrm{Re}[0.8Z_L(H)+0.2Z_R(H)]. \tag{52}$$

The theoretical $R(H)$, which includes effects from both the tilted cylinder and the heterodyne gaps, is shown in Fig. 5. The agreement with the experimental data of Fig. 1 is remarkable.

IV. CONCLUSION

Inspection of Figs. 1–5 allows one to recognize that the CDW in potassium[6–8] has profound consequences in studies of the perpendicular-field cyclotron resonance. The fact that cyclotron resonance even exists (in the surface resistance, R vs H) attests to the presence of the small Fermi-surface cylinder (the dark areas of Fig. 2), created by the CDW gap and the first minigap. A theory based on only a spherical Fermi surface does not allow any structure near $\omega_c=\omega$, as shown by the top curve of Fig. 1.

The shape of the $R(H)$ resonance (compare Figs. 4 and 5) reveals that the cylinder's axis is tilted away from [110] (the field direction) by $\sim 45°$, as was found theoretically.[14,8] (The reason for the tilt is to minimize the elastic-stress energy involved in creating the periodic lattice distortion, of wave vector $\vec{G}_{110}-\vec{Q}$, needed to screen the electronic CDW.[14])

The drop in R for $|H|>|H_c|$, see Fig. 3 and the experimental data of Fig. 1, arises from the heterodyne gaps (Fig. 2), which interrupt the cyclotron motion of equatorial orbits, and cause a partial loss in carrier effectiveness.

The volume of the Fermi-surface cylinder (corresponding to $\eta=4\times10^{-4}$ electrons/atom) was determined from the size of the resonance relative to $R(H_c)-R(0)$.[10] The fact that this volume equals the product of the cylinder's length (along [110]), determined from $\vec{Q}$ (observed in neutron diffraction[15]) and the cylinder's cross section (perpendicular to [110]), defined by the periodicity of Landau-level oscillations observed in microwave transmission,[12] indicates a com-

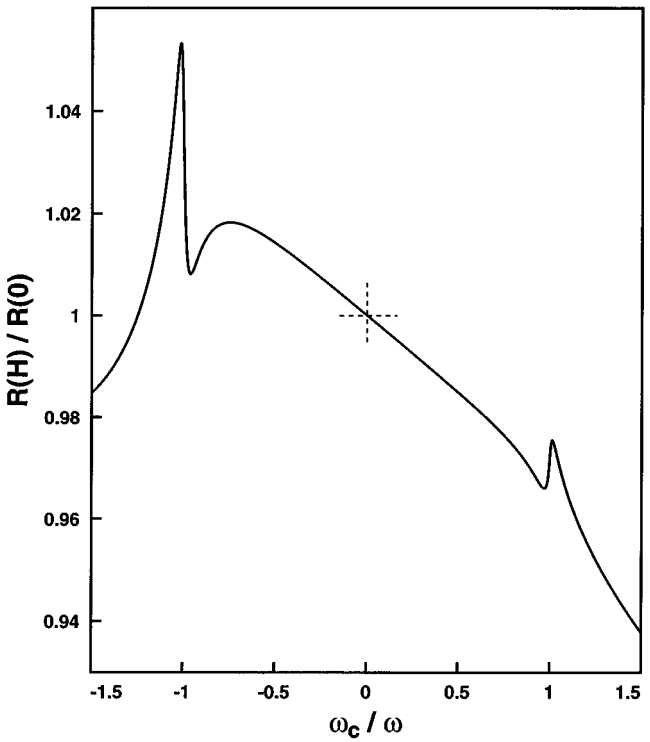

FIG. 5. Theoretical $R(H)$ for potassium based on the heterodyne-gap parameters of Fig. 3 and the Fermi-surface cylinder model of Fig. 4, except that the cylinder's axis is tilted 45° from [110]. [The tilt is required to minimize the elastic stress of the periodic lattice distortion needed to neutralize the electronic CDW (Ref. 14).] This calculated behavior should be compared with Baraff, Grimes, and Platzman's data in Fig. 1.

pelling consistency among relevant phenomena.

Fracture of potassium's Fermi surface by CDW minigaps and heterodyne gaps, Fig. 2, is not only evident in the surface resistance anomalies studied here, but is the cause of many other magnetotransport effects, the most spectacular of which are the multitudinous open-orbit resonances[21] created by the minigaps and heterodyne gaps. These open-orbit spectra have been explained within the same framework employed here.[17] Without a broken symmetry, potassium would be the simplest metal of all since, unlike Li (Ref. 22) or Na, it would retain its cubic symmetry to helium temperature. However, as a consequence of its CDW, potassium has provided (during the last 33 years) a veritable universe of unanticipated behavior—a challenge to all who seek to understand electrons in metals.

ACKNOWLEDGMENTS

The authors are indebted to the National Science Foundation, Division of Materials Research for support. We are grateful to Graciela Lacueva and C.C. Grimes for helpful discussions. Dr. Grimes kindly provided original data, including perpendicular-field resonance and Azbel-Kaner (A-K) oscillations on the same specimen. The A-K oscillations usually had five subharmonics, consistent with theory[3] for $\omega\tau\sim 30$, throughout the skin depth.

APPENDIX A: CALCULATION OF THE CONDUCTIVITY

Equation (6) can be rearranged as follows:

$$f_{\rm eff}(k_z)=\frac{f+(1-f)e^{-H_0/H}+1-1+\beta|t|}{1+\beta|t|}$$
$$=1+\frac{(1-f)(e^{-H_0/H}-1)}{1+\beta|t|}. \tag{A1}$$

From Eqs. (7) and (9) we have expressions for σ_{xx} and σ_{xy},

$$\sigma_{xx}=\frac{3\sigma_0}{8}\int_{-1}^{1}dt(1-t^2)\left[1+\frac{f+(1-f)e^{-H_0/H}-1}{1+\beta|t|}\right]$$
$$\times\left[\frac{1}{1-ia_++ixt}+\frac{1}{1-ia_-+ixt}\right]$$
$$=\sigma_{xx}^{\rm orig}+[f+(1-f)e^{-H_0/H}-1]\sigma'_{xx}, \tag{A2}$$

$$\sigma_{xy}=\frac{3i\sigma_0}{8}\int_{-1}^{1}dt(1-t^2)\left[1+\frac{f+(1-f)e^{-H_0/H}-1}{1+\beta|t|}\right]$$
$$\times\left[\frac{1}{1-ia_++ixt}-\frac{1}{1-ia_-+ixt}\right]$$
$$=\sigma_{xy}^{\rm orig}+[f+(1-f)e^{-H_0/H}-1]\sigma'_{xy}, \tag{A3}$$

where

$$\sigma'_{xx}=\frac{3\sigma_0}{8}\int_{-1}^{1}dt\,\frac{1-t^2}{1+\beta|t|}\left[\frac{1}{1-ia_++ixt}+\frac{1}{1-ia_-+ixt}\right],$$

$$\sigma'_{xy}=\frac{3i\sigma_0}{8}\int_{-1}^{1}dt\,\frac{1-t^2}{1+\beta|t|}\left[\frac{1}{1-ia_++ixt}-\frac{1}{1-ia_-+ixt}\right], \tag{A4}$$

and $\sigma_{xx}^{\rm orig}$ and $\sigma_{xy}^{\rm orig}$ are the same as σ_{xx} and σ_{xy} in Eq. (7). These expressions were evaluated previously,[10]

$$\sigma_{xx}^{\rm orig}=\frac{3\sigma_0}{4x^2}\{2a_+p_++2a_-p_--2+r_+(x^2+1-a_+^2)+r_-(x^2$$
$$+1-a_-^2)+i[a_++a_-+p_+(x^2+1-a_+^2)$$
$$-p_-(x^2+1-a_-^2)-2a_+r_+-2a_-r_-]\},$$

$$\sigma_{xy}^{\rm orig}=\frac{3\sigma_0}{4x^2}\{a_--a_++p_-(x^2+1-a_-^2)-p_+(x^2+1-a_+^2)$$
$$+2a_+r_+-2a_-r_-+i[2a_+p_+-2a_-p_-$$
$$+r_+(x^2+1-a_+^2)-r_-(x^2+1-a_-^2)]\}, \tag{A5}$$

where

$$a_\pm=(\omega\pm\omega_c)\tau, \tag{A6}$$

$$x=ql,$$

$$p_\pm=\frac{1}{4x}\ln\left[\frac{1+(x+a_\pm)^2}{1+(x-a_\pm)^2}\right],$$

$$r_{\pm}=\frac{1}{2x}[\tan^{-1}(x+a_{\pm})+\tan^{-1}(x-a_{\pm})].$$

Integration of Eq. (A3) is tedious but straightforward. The final forms are

$$\begin{aligned}\sigma_{xx}=&\frac{3\sigma_0}{4x^2}\{2a_+p_+ +2a_-p_- -2+r_+(x^2+1-a_+^2)+r_-(x^2+1-a_-^2)+[f+(1-f)e^{-H_0/H}-1]\\&\times[x(f_+-f'_+ +f_- -f'_-)-\beta a_+(f_+ +f'_+)-\beta a_-(f_- +f'_-)-\beta(g_+ +g'_+ +g_- +g'_-)+(s_+ +s'_+ +s_- +s'_-)x^2]\\&+i[a_+ +a_- +p_+(x^2+1-a_+^2)+p_-(x^2+1-a_-^2)-2a_+r_+ -2a_-r_-]+i[f+(1-f)e^{-H_0/H}-1]\\&\times[x(g_+ -g'_+ +g_- -g'_-)-\beta a_+(g_+ +g'_+)-\beta a_-(g_- +g'_-)+\beta(f_+ +f'_+ +f_- +f'_-)+(t_+ +t'_+ +t_- +t'_-)x^2]\},\end{aligned}$$

$$\begin{aligned}\sigma_{xy}=&\frac{3\sigma_0}{4x^2}\{a_- -a_+ +p_-(x^2+1-a_-^2)-p_+(x^2+1-a_+^2)+2a_+r_+ -2a_-r_-+[f+(1-f)e^{-H_0/H}-1][x(g_- -g'_- -g_+ +g'_+)\\&+\beta a_+(g_+ +g'_+)-\beta a_-(g_- +g'_-)+\beta(f_- +f'_- -f_+ -f'_+)+(t_- +t'_- -t_+ -t'_+)x^2]+i[2a_+p_+ -2a_-p_- -r_-(x^2+1\\&-a_-^2)+r_+(x^2+1-a_+^2)]+i[f+(1-f)e^{-H_0/H}-1][x(f_+ -f'_+ -f_- +f'_-)-\beta a_+(f_+ +f'_+)\\&+\beta a_-(f_- +f'_-)-\beta(g_+ +g'_+ -g_- -g'_-)+(s_+ +s'_+ -s_- -s'_-)x^2]\},\end{aligned}\tag{A7}$$

where

$$u_{\pm}=\frac{1}{2}\ln\left[\frac{1+a_{\pm}^2}{1+(x+a_{\pm})^2}\right],$$

$$v_{\pm}=\tan^{-1}(x+a_{\pm})-\tan^{-1}(a_{\pm}),$$

$$f_{\pm}=\frac{1}{2}\frac{1}{\beta^2+(x-\beta a_{\pm})^2}[-2a_{\pm}u_{\pm}-v_{\pm}(a_{\pm}^2-x^2-1)-x],$$

$$g_{\pm}=\frac{1}{2}\frac{1}{\beta^2+(x-\beta a_{\pm})^2}\left[-2a_{\pm}v_{\pm}+u_{\pm}(a_{\pm}^2-x^2-1)-\frac{x(x-2a_{\pm})}{2}\right],$$

$$s_{\pm}=\frac{1}{2}\frac{\beta^2}{\beta^2+(x-\beta a_{\pm})^2}\left[\left(\frac{1}{\beta}-\frac{1}{\beta^3}\right)\ln(1+\beta)+\frac{1}{\beta^2}\left(1-\frac{\beta}{2}\right)\right],$$

$$t_{\pm}=\frac{1}{2}\frac{-\beta(x-\beta a_{\pm})}{\beta^2+(x-\beta a_{\pm})^2}\left[\left(\frac{1}{\beta}-\frac{1}{\beta^3}\right)\ln(1+\beta)+\frac{1}{\beta^2}\left(1-\frac{\beta}{2}\right)\right].\tag{A8}$$

Furthermore, $f'_{\pm}(x)=f_{\pm}(-x)$, $g'_{\pm}(x)=g_{\pm}(-x)$, $s'_{\pm}(x)=s_{\pm}(-x)$, and $t'_{\pm}(x)=t_{\pm}(-x)$. The foregoing results are to be used in the integrand of Eq. (22), which must then be evaluated numerically.

APPENDIX B: POLARIZATION OF THE FIELD INSIDE AN ANISOTROPIC METAL

Consider a metal in a high-frequency electromagnetic field. To learn how the wave is polarized we shall treat the normal skin effect for which Ohm's law, $\vec{j}=\sigma\vec{E}$, is valid and the conductivity is local. The relevant Maxwell equations are

$$\vec{\nabla}\times\vec{\mathcal{E}}=-\frac{1}{c}\frac{\partial\vec{H}}{\partial t},$$

$$\vec{\nabla}\times\vec{H}=\frac{4\pi}{c}\vec{j}.\tag{B1}$$

We neglect the displacement current. Let us assume that the metal fills the $z>0$ half space, and that the wave is incident normal to the surface. For a wave propagating in the z direction we shall seek a solution proportional to $\exp(iqz-i\omega t)$. Eliminating the magnetic field $\vec{H}$ from Eq. (B1), we can easily find:

$$-\nabla^2\vec{\mathcal{E}}+\vec{\nabla}(\vec{\nabla}\cdot\vec{\mathcal{E}})+\frac{4\pi}{c^2}\frac{\partial}{\partial t}\vec{j}=0,\tag{B2}$$

which reduces to

$$\frac{\partial^2}{\partial z^2}\mathcal{E}_{\alpha}+\frac{4\pi i\omega}{c^2}j_{\alpha}=0,\tag{B3}$$

$$j_z=0, \tag{B4}$$

where $\alpha=x,y$. The conductivity of a nearly-free-electron system in the local approximation is

$$\sigma^s=\frac{ne^2\tau}{m^*}\frac{1}{(1-i\omega\tau)^2+(\omega_c\tau)^2}\begin{pmatrix} 1-i\omega\tau & -\omega_c\tau & 0 \\ \omega_c\tau & 1-i\omega\tau & 0 \\ 0 & 0 & \dfrac{(1-i\omega\tau)^2+(\omega_c\tau)^2}{1-i\omega\tau} \end{pmatrix}. \tag{B5}$$

The conductivity of the Fermi-surface cylinder, as calculated in Sec. III, is

$$\sigma^c=\frac{\eta ne^2\tau_c}{m^*}\frac{1}{(1-i\omega\tau_c)^2+(\omega_c\tau_c)^2}\begin{pmatrix} 1-i\omega\tau_c & -\omega_c\tau_c & -\tan\theta(1-i\omega\tau_c) \\ \omega_c\tau_c & 1-i\omega\tau_c & -\tan\theta(\omega_c\tau_c) \\ -\tan\theta(1-i\omega\tau_c) & \tan\theta(\omega_c\tau_c) & \tan^2\theta(1-i\omega\tau_c) \end{pmatrix}. \tag{B6}$$

The total conductivity is $\sigma^s+\sigma^c$. The usual expression for the conductivity tensor is

$$\sigma=\begin{pmatrix} \sigma_{xx} & \sigma_{xy} & \sigma_{xz} \\ \sigma_{yx} & \sigma_{yy} & \sigma_{yz} \\ \sigma_{zx} & \sigma_{zy} & \sigma_{zz} \end{pmatrix}. \tag{B7}$$

Because the number of electrons enclosed by the cylindrical Fermi surface is only a fraction, $\eta=4\times10^{-4}$, of the total, the following inequalities prevail:

$$\sigma_{xz},\sigma_{yz},\sigma_{zx},\sigma_{zy}\ll\sigma_{xx},\sigma_{yy},\sigma_{zz},\sigma_{xy},\sigma_{yx}. \tag{B8}$$

Using Ohm's law to express Eqs. (B3) and (B4), we find a set of homogeneous equations:

$$\left(q^2-\frac{4\pi i\omega}{c^2}\sigma_{xx}\right)\mathcal{E}_x-\frac{4\pi i\omega}{c^2}\sigma_{xy}\mathcal{E}_y-\frac{4\pi i\omega}{c^2}\sigma_{xz}\mathcal{E}_z=0,$$

$$-\frac{4\pi i\omega}{c^2}\sigma_{yx}\mathcal{E}_x+\left(q^2-\frac{4\pi i\omega}{c^2}\sigma_{yy}\right)\mathcal{E}_y-\frac{4\pi i\omega}{c^2}\sigma_{yz}\mathcal{E}_z=0,$$

$$\sigma_{zx}\mathcal{E}_x+\sigma_{zy}\mathcal{E}_y+\sigma_{zz}\mathcal{E}_z=0. \tag{B9}$$

We next eliminate $\mathcal{E}_z$ in favor of $\mathcal{E}_x$ and $\mathcal{E}_y$, using the third equation of (B9). This allows us to express (B9) with $\mathcal{E}_x$ and $\mathcal{E}_y$ only:

$$\left(q^2-\frac{4\pi i\omega}{c^2}\sigma'_{xx}\right)\mathcal{E}_x-\frac{4\pi i\omega}{c^2}\sigma'_{xy}\mathcal{E}_y=0,$$

$$-\frac{4\pi i\omega}{c^2}\sigma'_{yx}\mathcal{E}_x+\left(q^2-\frac{4\pi i\omega}{c^2}\sigma'_{yy}\right)\mathcal{E}_y=0, \tag{B10}$$

where

$$\sigma'_{\alpha\beta}=\sigma_{\alpha\beta}-\frac{\sigma_{\alpha z}\sigma_{z\beta}}{\sigma_{zz}}. \tag{B11}$$

Here α and β indicate x or y components only. This change of $\sigma_{\alpha\beta}$ to $\sigma'_{\alpha\beta}$ is the main contribution of the electrons in the tilted cylinder. Transverse conductivities are mixed with longitudinal conductivity on account of the longitudinal motion of electrons in the cylinder. The determinant of (B10) must vanish; and this condition leads to the allowed propagation vectors:

$$q_1^2=\frac{1}{2}\frac{4\pi i\omega}{c^2}[\sigma'_{xx}+\sigma'_{yy}+\sqrt{(\sigma'_{xx}-\sigma'_{yy})^2+4\sigma'_{xy}\sigma'_{yx}}],$$

$$q_2^2=\frac{1}{2}\frac{4\pi i\omega}{c^2}[\sigma'_{xx}+\sigma'_{yy}-\sqrt{(\sigma'_{xx}-\sigma'_{yy})^2+4\sigma'_{xy}\sigma'_{yx}}]. \tag{B12}$$

Therefore the two electric-field modes are

$$\vec{\mathcal{E}}_1=\mathcal{E}_{10}\left\{\hat{x}+\frac{q_1^2c^2-4\pi i\omega\sigma'_{xx}}{4\pi i\omega\sigma'_{xy}}\hat{y}-\left[\frac{(q_1^2c^2-4\pi i\omega\sigma'_{xx})\sigma_{zy}+4\pi i\omega\sigma'_{xy}\sigma_{zx}}{4\pi i\omega\sigma'_{xy}\sigma_{zz}}\right]\hat{z}\right\}e^{iq_1z-i\omega t},$$

$$\vec{\mathcal{E}}_2=\mathcal{E}_{20}\left\{\hat{x}+\frac{q_2^2c^2-4\pi i\omega\sigma'_{xx}}{4\pi i\omega\sigma'_{xy}}\hat{y}-\left[\frac{(q_2^2c^2-4\pi i\omega\sigma'_{xx})\sigma_{zy}+4\pi i\omega\sigma'_{xy}\sigma_{zx}}{4\pi i\omega\sigma'_{xy}\sigma_{zz}}\right]\hat{z}\right\}e^{iq_2z-i\omega t}. \tag{B13}$$

The amplitudes of the transmitted wave, $\mathcal{E}_{10}$ and $\mathcal{E}_{20}$, can be obtained in terms of the amplitudes of the incident wave $\vec{\mathcal{E}}^{\,I}$ by requiring the tangential field components to be continuous at the boundary. There are incident, reflected, and transmitted electric fields on the surface $z=0$:

$$\vec{\mathcal{E}}^{\,I}=(\mathcal{E}^{\,I}_x\hat{x}+\mathcal{E}^{\,I}_y\hat{y})e^{iq_0z-i\omega t},$$

$$\vec{\mathcal{E}}^{\,R}=(\mathcal{E}^{\,R}_x\hat{x}+\mathcal{E}^{\,R}_y\hat{y}+\mathcal{E}^{\,R}_z\hat{z})e^{-iq_0z-i\omega t},$$

$$\vec{\mathcal{E}}^{\,T}=\mathcal{E}_{10}(\hat{x}+\alpha_1\hat{y}+\beta_1\hat{z})e^{iq_1z-i\omega t}+\mathcal{E}_{20}(\hat{x}+\alpha_2\hat{y}+\beta_2\hat{z})e^{iq_2z-i\omega t}, \tag{B14}$$

where I indicates the incident wave propagating along $\hat{z}$ with wave vector $q_0=\omega/c$, R indicates the reflected wave traveling along $-\hat{z}$ with wave vector $-q_0$, and T indicates the transmitted wave. Equation (B1) requires the microwave magnetic field to have x and y components only:

$$\vec{H}^I=(\mathcal{E}^I_y\hat{x}+\mathcal{E}^I_x\hat{y})e^{iq_0z-i\omega t},$$

$$\vec{H}^R=(\mathcal{E}^R_y\hat{x}-\mathcal{E}^R_x\hat{y})e^{-iq_0z-i\omega t},$$

$$\vec{H}^T=\frac{\mathcal{E}_{10}q_1}{q_0}(-\alpha_1\hat{x}+\hat{y})e^{iq_1z-i\omega t}+\frac{\mathcal{E}_{20}q_2}{q_0}(-\alpha_2\hat{x}+\hat{y})e^{iq_2z-i\omega t}, \tag{B15}$$

where

$$\alpha_i=\frac{q_i^2c^2-4\pi i\omega\sigma'_{xx}}{4\pi i\omega\sigma'_{xy}},$$

$$\beta_i=-\frac{(q_i^2c^2-4\pi i\omega\sigma'_{xx})\sigma_{zy}+4\pi i\omega\sigma'_{xy}\sigma_{zx}}{4\pi i\omega\sigma'_{xy}\sigma_{zz}}. \tag{B16}$$

For the purposes of this appendix we treat potassium as a nearly-free-electron gas characterized by the following parameters: effective mass $m^*=1.21m$, electron density $n=1.4\times10^{22}$ cm^{-3}, Fermi radius $k_F=0.75\times10^8$ cm^{-1}, and electron scattering time $\tau=2.0\times10^{-10}$ s (which is appropriate at $T=2.5$ K). The frequency of the applied microwave field is 23.9 GHz. Accordingly, $\omega\tau=30$ is used for electrons on the spherical Fermi-surface. On account of the small velocity for electrons in the Fermi-surface cylinder $\omega\tau_c=150$. (This value is required to fit the observed width of the cyclotron-resonance peak in Fig. 1.)

The inequalities of Eq. (B8) are so extreme that α_1 and α_2 differ from i and $-i$ by $\sim10^{-6}$. Specifically,

$$\alpha_1\approx i,$$

$$\alpha_2\approx -i. \tag{B17}$$

The ratio of the x or y component to the z component is about 100, so

$$\mathcal{E}^T_x,\mathcal{E}^T_y\gg\mathcal{E}^T_z. \tag{B18}$$

Calculation of $\mathcal{E}_{10}$ and $\mathcal{E}_{20}$ is straightforward by using the continuity of the tangential field at $z=0$. The final results are

$$\mathcal{E}_{10}=\frac{-2q_0}{(\alpha_1-\alpha_2)(q_0+q_1)}(\alpha_2\mathcal{E}^I_x-\mathcal{E}^I_y), \tag{B19}$$

$$\mathcal{E}_{20}=\frac{2q_0}{(\alpha_1-\alpha_2)(q_0+q_2)}(\alpha_1\mathcal{E}^I_x-\mathcal{E}^I_y).$$

The amplitude of the transmitted wave may be found by specifying the incident wave. For right-circular polarization,

$$\mathcal{E}^I_y=i\mathcal{E}^I_x. \tag{B20}$$

On account of the extreme inequality (B8), one mode dominates the other by a factor of at least 10^7 for all magnetic fields, i.e.,

$$\mathcal{E}_{10}\gg\mathcal{E}_{20}. \tag{B21}$$

For left-circular polarization,

$$\mathcal{E}^I_y=-i\mathcal{E}^I_x, \tag{B22}$$

and $\mathcal{E}_{20}$ is much larger than $\mathcal{E}_{10}$.

The magnetic field at $z=0$ can be found from Eq. (B15):

$$H_x(0)=\frac{2\alpha_1q_1(\alpha_2\mathcal{E}^I_x-\mathcal{E}^I_y)}{(\alpha_1-\alpha_2)(q_0+q_1)}-\frac{2\alpha_2q_2(\alpha_1\mathcal{E}^I_x-\mathcal{E}^I_y)}{(\alpha_1-\alpha_2)(q_0+q_2)},$$

$$H_y(0)=\frac{-2q_1(\alpha_2\mathcal{E}^I_x-\mathcal{E}^I_y)}{(\alpha_1-\alpha_2)(q_0+q_1)}+\frac{2q_2(\alpha_1\mathcal{E}^I_x-\mathcal{E}^I_y)}{(\alpha_1-\alpha_2)(q_0+q_2)}. \tag{B23}$$

From Eq. (B17) and the fact that $q_1,q_2\gg q_0$, the magnetic field at the surface is

$$H_x(0)\approx\mp2i\mathcal{E}^I_x \quad \text{for} \quad \mathcal{E}^I_y=\pm i\mathcal{E}^I_x,$$

$$H_y(0)\approx2\mathcal{E}^I_x \quad \text{for} \quad \mathcal{E}^I_y=\pm i\mathcal{E}^I_x. \tag{B24}$$

Therefore the total current defined by Eq. (40) is

$$J_x=\frac{c}{4\pi}H_y(0)\approx\frac{c}{2\pi}\mathcal{E}^I_x,$$

$$J_y=-\frac{c}{4\pi}H_x(0)\approx\pm i\frac{c}{2\pi}\mathcal{E}^I_x. \tag{B25}$$

The foregoing results are incorporated in the calculations of Sec. III at Eqs. (43) and (44). It must be appreciated that the Fermi-sphere electrons are treated nonlocally in Sec. III. The purpose of this appendix is to show that the microwave modes in the metal are essentially circularly polarized (despite the broken axial symmetry caused by the tilt of the Fermi-surface cylinder) on account of the small value (4×10^{-4}) of η.

[1] C. C. Grimes and A. F. Kip, Phys. Rev. **132**, 1991 (1963).
[2] M. Ya. Azbel and E. A. Kaner, Zh. Éksp. Teor. Fiz. **32**, 896 (1957) [Sov. Phys. JETP **5**, 730 (1957)].
[3] D. C. Mattis and G. Dresselhaus, Phys. Rev. **111**, 403 (1958).
[4] R. G. Chambers, Philos. Mag. **1**, 459 (1965).
[5] G. A. Baraff, C. C. Grimes, and P. M. Platzman, Phys. Rev. Lett. **22**, 590 (1969).
[6] A. W. Overhauser, Phys. Rev. **167**, 691 (1968).
[7] A. W. Overhauser, Adv. Phys. **27**, 343 (1978); in *Highlights of Condensed-Matter Theory*, Proceedings of the International

School of Physics ''Enrico Fermi,'' Course LXXXIX, Varenna on Lake Como, 1983, edited by F. Bassani, F. Fumi, and M. P. Tosi (North-Holland, Amsterdam, 1985), p. 194.
[8] Yong Gyoo Hwang and A. W. Overhauser, Phys. Rev. B **39**, 3037 (1989).
[9] A. W. Overhauser and N. R. Butler, Phys. Rev. B **14**, 3371 (1976).
[10] G. Lacueva and A. W. Overhauser, Phys. Rev. B **33**, 3765 (1986).
[11] G. L. Dunifer, J. F. Sambles, and D. A. H. Mace, J. Phys. Condens. Matter **1**, 875 (1989).
[12] Graciela Lacueva and A. W. Overhauser, Phys. Rev. B **46**, 1273 (1992).
[13] C. C. Grimes (private communication).
[14] G. F. Giuliani and A. W. Overhauser, Phys. Rev. B **20**, 1328 (1979).
[15] T. M. Giebultowicz, A. W. Overhauser, and S. A. Werner, Phys. Rev. Lett. **56**, 2228 (1986); Phys. Rev. B **41**, 12 536 (1990).
[16] E. I. Blount, Phys. Rev. **126**, 1636 (1962).
[17] M. Huberman and A. W. Overhauser, Phys. Rev. B **25**, 2211 (1982).
[18] C. Kittel, *Quantum Theory of Solids* (John Wiley and Sons, New York, 1963), p. 313.
[19] P. A. Penz and T. Kushida, Phys. Rev. **176**, 804 (1968).
[20] G. A. Baraff, Phys. Rev. **187**, 851 (1969), first paragraph.
[21] P. G. Coulter and W. R. Datars, Can. J. Phys. **63**, 159 (1985).
[22] A. W. Overhauser, Phys. Rev. Lett. **53**, 64 (1984).